Journal of Optics

ACCEPTED MANUSCRIPT

Modelling of the backside pattern transfer in magic mirror (Makyoh) imaging

To cite this article before publication: Ferenc Riesz 2022 *J. Opt.* in press https://doi.org/10.1088/2040-8986/aca98c

Manuscript version: Accepted Manuscript

Accepted Manuscript is "the version of the article accepted for publication including all changes made as a result of the peer review process, and which may also include the addition to the article by IOP Publishing of a header, an article ID, a cover sheet and/or an 'Accepted Manuscript' watermark, but excluding any other editing, typesetting or other changes made by IOP Publishing and/or its licensors"

This Accepted Manuscript is **© 2022 IOP Publishing Ltd**.

During the embargo period (the 12 month period from the publication of the Version of Record of this article), the Accepted Manuscript is fully protected by copyright and cannot be reused or reposted elsewhere.
As the Version of Record of this article is going to be / has been published on a subscription basis, this Accepted Manuscript is available for reuse under a CC BY-NC-ND 3.0 licence after the 12 month embargo period.

After the embargo period, everyone is permitted to use copy and redistribute this article for non-commercial purposes only, provided that they adhere to all the terms of the licence https://creativecommons.org/licences/by-nc-nd/3.0

Although reasonable endeavours have been taken to obtain all necessary permissions from third parties to include their copyrighted content within this article, their full citation and copyright line may not be present in this Accepted Manuscript version. Before using any content from this article, please refer to the Version of Record on IOPscience once published for full citation and copyright details, as permissions will likely be required. All third party content is fully copyright protected, unless specifically stated otherwise in the figure caption in the Version of Record.

View the article online for updates and enhancements.

This content was downloaded from IP address 176.63.12.162 on 14/12/2022 at 14:28

IOP Publishing Journal Title
Journal **XX** (XXXX) XXXXXX https://doi.org/XXXX/XXXX

Modelling of the backside pattern transfer in magic mirror (Makyoh) imaging

Ferenc Riesz

Centre for Energy Research, Institute for Technical Physics and Materials Science, P. O. Box 49, H–1525 Budapest, Hungary

E-mail: riesz.ferenc@ek-cer.hu

Received xxxxxx
Accepted for publication xxxxxx
Published xxxxxx

Abstract

A model of magic-mirror (Makyoh) imaging with the mirror backside relief as the input is described. The mechanical pattern transfer is modelled by a convolution approach while the optical imaging using a nonlinear geometrical optical model, more general than previous approaches. Characteristic features of the imaging is analysed and the linear approximation is examined. Diffraction effects are also treated. Characteristic features for the ancient mirror and applications in semiconductor wafer inspection are discussed.

Keywords: Makyoh, geometrical optics, optical imaging, optical inspection

1. Introduction

Oriental magic mirrors (‘Makyoh’, after their Japanese name) [1, 2] have received much interest from the optics community since the 19th century [3-6]. Such a mirror is an essentially flat or slightly convex mirror made of bronze with a backside relief pattern. Projecting a parallel light beam (e.g. sunshine) onto the front surface, a reflected image corresponding to the back pattern appears on a distant screen, giving the illusion of transparency of the mirror. The explanation of this ‘magic’ property is based on backside pattern transfer: the back relief translates to the polished front face as a nearly invisible surface relief during the machining of the mirror. The concave (convex) regions of this relief then focus (defocus) the reflected beam, thus causing contrast variations in the image. The correspondence between back relief and the Makyoh image has been experimentally confirmed [7].

An increased interest in this phenomenon arose in the 1990s because of the principle’s application as a powerful topographic tool (Makyoh topography) for the qualitative inspection of the surface defects and texture of semiconductor wafers and other nearly flat, mirror-like surfaces [8-10]. In these applications, the backside pattern transfer is one possible cause of the front surface relief. For example, in wafer polishing, a contaminant particle on the backside causes a mound on the front face. This mound is then polished to be flat which causes a depression when the wafer is released from the chuck [8]. Interface particles or bubbles cause outer-face deformations during wafer bonding [9]. Similar mechanisms, that is, surface deformations caused by localised buried stressors are often accounted for various phenomena in materials technology [11, 12].

Using modern fabrication tools with controlled parameters, backside pattern transfer can be utilised as a novel machining method. Magic mirror model replicas, showing the “magic” imaging properties of the ancient mirror, have been fabricated by boring a pattern onto the backside of a metal disc then polishing its front face [13, 14]. Submicron wavy textures on a flat metal surface were realised by forming a back relief pattern then thinning down the workpiece using diamond turning [15].

That is, magic mirror imaging appears to be a universal mechanism related to diverse areas involving a mechanical pattern transfer and an optical imaging step. Efforts to quantitatively model the image forming as a function of

Accepted Manuscript

 © xxxx IOP Publishing Ltd

backside relief have however been limited. Berry discussed the Makyoh imaging of a straight backside surface step using an approximate (linear) imaging model [3]. He treated the pattern transfer process as smoothing the abrupt step into the error function. In their comment to Berry's paper, the authors in [16] proposed the hyperbolic tangent function instead. Gitin used linear system theory for arbitrary back relief patterns by considering a Dirac delta-like backside 'excitation' and determined a simplified spatial impulse response of the system [4]. Both authors however considered a simplified, linear model of Makyoh image formation, therefore their results are applicable only in a limited range of imaging.

In this paper, we present an improved model describing the imaging with the backside profile as an input. We utilise the above ideas developed by Berry and Gitin, but use a more advanced model of Makyoh imaging and examine the imaging properties more deeply, with an aim the find the pivoting parameters of the backside pattern transfer process and look at their influence on the imaging. Relevance to the ancient magic mirrors and to the problems in semiconductor technology are also discussed.

2. Model formulation

2.1 Summary of the geometrical optical model of Makyoh imaging

The geometrical optical model of Makyoh imaging has been described in [5] in detail. For a closely plane surface, parallel illuminating beam and unity surface reflectivity, the model consists of two equations:

$$\boldsymbol{f}(\boldsymbol{r}) = r - 2L\ grad\ h(\boldsymbol{r}) \qquad (1)$$

and

$$I(\boldsymbol{f}) = \frac{1}{|1-4LH(\boldsymbol{r})+4L^2K(\boldsymbol{r})|}, \qquad (2)$$

where $h(\boldsymbol{r})$ is the surface height profile, $\boldsymbol{r}$ is the spatial co-ordinate in the mirror plane, $\boldsymbol{f}$ is the same in the image plane, and L is the distance between screen and mirror; I is the relative image intensity referenced to that of a flat surface, and H and K are the mean and Gaussian curvatures of the mirror surface, respectively. As the angular deflections of the reflected rays are small, the factors due to non-normal incidence and reflection are neglected. The condition $1/I(\boldsymbol{f}) = 0$ in the screen plane gives the equation of the caustic curve. This happens above a certain $|L|$ for a given surface. In the non-caustic region of L, the image of any two non-overlapping surface area does not overlap, that is, the surface topology is preserved in the image [5]. In the caustic regime, the topological connection between the surface and the image is lost, therefore this region is usually avoided. In the following, we also deal with the non-caustic region only. The absolute sign in equation (2) in this case can be dropped.

Note that L can also be made negative by using special optical arrangements.

Equation (1) represents a mapping of the surface plane onto the image plane according to the surface gradients, while equation (2) gives the intensity of the image points in terms of the local surface curvatures. Note that the intensities are given in the image plane points $\boldsymbol{f}$ as mapped by equation (1), but are expressed with the curvatures in the mirror plane points $\boldsymbol{r}$.

The imaging is essentially non-linear [17]. The non-linearity is caused by the above-mentioned mapping as well as the Gaussian-curvature related term in equation (2). The degree of the non-linearity can be expressed by the ratio of the Gaussian to the mean curvature related terms as $-LK/H$.

If L is much smaller than the local surface curvature radii, the image intensity can be approximated by the Laplacian of the surface relief pattern [3, 18] as

$$I(\boldsymbol{f}) = \frac{1}{1-2L\Delta h(\boldsymbol{r})}. \qquad (3)$$

This can be rearranged as linear if the intensity is transformed as $1-1/I$. However, equation (3) can also be approximated further as:

$$I(\boldsymbol{f}) = 1 + 2L\Delta h(\boldsymbol{r}). \qquad (4)$$

The basis of the approximation is neglecting the higher-than-first-order terms of the surface derivatives in the expression of the intensity [18]. (Berry [3] obtained the same formula as equation (4) in a different way.) This leads to dropping the Gaussian curvature related term in equation (2). It also implies that equation (3) is valid not only if the curvatures are small, but in all cases when $K = 0$, that is, in cylindrical surfaces or surfaces with translational symmetry. Another approximation is neglecting the surface mapping, that is, $\boldsymbol{f}(\boldsymbol{r}) = \boldsymbol{r}$ is taken. This leads to easily manageable expressions in equations (3) and (4). This approximation can usually be performed if the surface is overall flat and the deviations from the flatness are limited in lateral size.

It is important to note that these two approximations can be applied independently, depending on the properties of the surface and on the image properties we are interested in, since, in general, they do not depend directly on each other. For example, if a slowly varying global surface shape is present but the local curvature radii are small compared to L, the Laplacian approximation can be applied but the gradient-related mapping cannot be neglected (this happens e.g. at the ancient mirrors as they are usually slightly convex).

2.2 Modelling of the backside pattern transfer

The fabrication of the ancient mirror involves first casting the mirror with the back relief pattern, then polishing the front surface while exerting a strong pressure on the mirror plate [1, 2]. During this process, the mirror bends, and the bending is easier where the mirror is thinner; that is, less material is removed from these regions. The thickness variations finally result in the front surface relief upon releasing the pressure,

Accepted Manuscript

e.g. a back-face protrusion will induce a corresponding front depression focusing the reflected beam resulting in a bright patch in the image. Figure 1 illustrates this process for a mirror having a back-side ridge and a step. (Berry notes [3] that the mirror he studied shows just opposite contrast. However, a large number of published images—back relief together with projected image—of original ancient [1, 2] as well as modern replica [13, 14] mirrors show contrast according to figure 1, so Berry's observation seems to be an exception and may indicate [17] another origin of the 'magic' property, such as uneven deformation related to the cooling after casting [19].)

As mentioned in the Introduction, Berry [3] treated the pattern transfer as a smoothing process where the backside abrupt step becomes the error function on the front face. This is equivalent to the convolution with a Gaussian function. The convolution approach was extended by Gitin to arbitrary back relief by considering a Dirac-delta excitation function [4] and, again, a Gaussian response function.

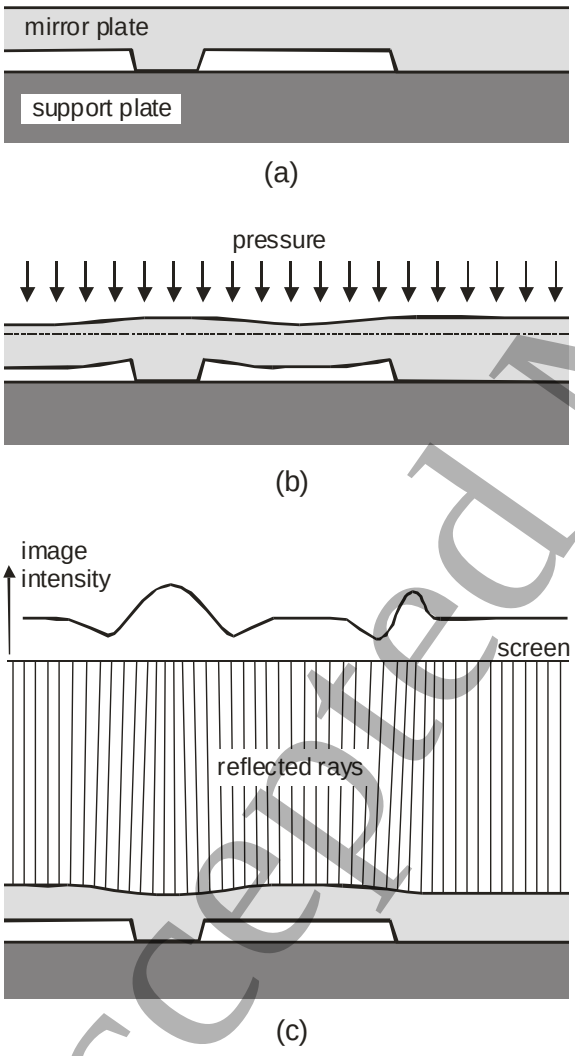

Figure 1. Scheme of the fabrication and imaging of the ancient magic mirror: (a) the cast mirror plate before polishing, (b) polishing under pressure, and (c) the ready mirror and the image formation

The related problem of the deformation of a semiconductor wafer due to small isolated backside particles during chucking was modelled by Bearda et al. [20]. The authors considered a point-like force exerted by the particle on a thin plate placed on a flat support and subjected to uniform pressure from the opposite side (figure 2). They defined the deflection length ρ_d, the radius around the excitation point, outside of which the wafer is in contact with the chuck. Using linear elasticity and standard thin-plate theory, the deflection $w(\rho)$ in the $0 < \rho \leq \rho_d$ region was given by [20]

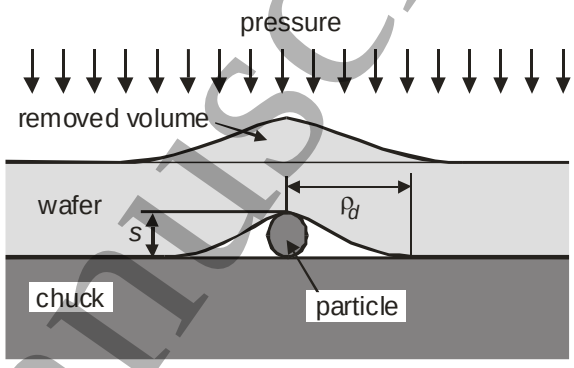

Figure 2. Formation of a mound during polishing of a semiconductor wafer due to a backside particle (see text for notation)

$$w(\rho) = s\left[1 - \left(\frac{\rho}{\rho_d}\right)^4 + 4\left(\frac{\rho}{\rho_d}\right)^2 ln\left(\frac{\rho}{\rho_d}\right)\right] \quad (5)$$

where s is the height of the particle and ρ is the distance from the excitation point. The value of ρ_d is given by [20]

$$\rho_d = \left(\frac{16E}{3(1-\nu)}\frac{st^3}{q}\right)^{1/4} \quad (6)$$

where E is the Young modulus, ν is the Poisson ratio, q is the pressure applied and t is the thickness of the wafer. The authors note that close to $\rho = 0$, formula (5) is invalid. Moreover, the particle itself may deform, or indent the wafer at the contact point. In practically realistic situations, ρ_d can extend to the mm range [20]. For our further analysis, it is reasonable to choose a Gaussian approximation of (6) because of its easy mathematical treatment and conforming to other studies. The Gaussian is often used to model small circular surface defects [5, 21] as well. The fit function can be written in the following normalised form, where A and d_n are the (dimensionless) fit parameters:

$$\frac{w_{fit}(\rho)}{s} = A\, exp\left(-\frac{(\rho/\rho_d)^2}{2{d_n}^2}\right). \quad (7)$$

Stipulating that $A = 1$ (which means that the front protrusion's height equals the particle height), we obtain a Gaussian fit with $d_n = 0.288$ for $\rho_d/10 \leq \rho \leq \rho_d$. Figure 3 shows the plots of equation (5) and the Gaussian fit. We can write (7) in a non-

Accepted Manuscript

normalised form as well, that is, use ρ as the argument and d as the usual Gaussian width parameter; then $d = \rho_d d_n$.

The case of the ancient mirror is more complicated because of the less definable problem and a higher role of plastic deformation in metals. Nevertheless, following [3] and [4] we keep the Gaussian function as a response to a point-like back excitation. The parameters depend on the plate thickness, material constants and the machining parameters. The value of A is much smaller than unity and decreases with increasing plate thickness, and d is in the order of two times the thickness (the width of the mound roughly equals twice the plate thickness assuming deformation spreading equally in all directions). Considering the fabrication process, a small amount of elastic deformation must be present to obtain a front relief, since if the deformation were entirely plastic, the mirror plate would not deform upon releasing of the polishing pressure. As the heights of the back relief pattern are in the mm range and the front deformation is submicron [22], A is in the order of one thousandth in real mirrors.

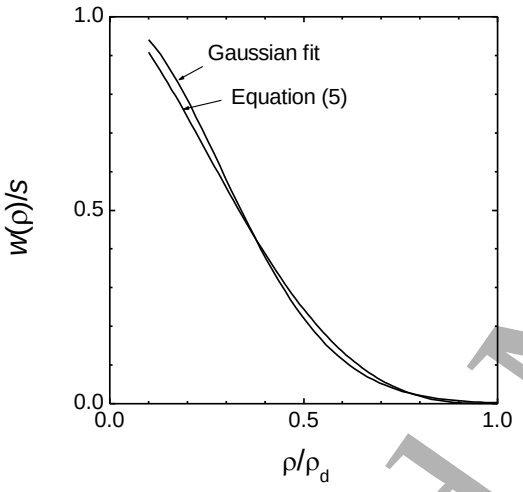

Figure 3. Plots of equation (5) and the Gaussian fit

In order to obtain the front profile for a continuous back height profile, a convolution approach can be applied, in line with the previous studies [4]. However, the process is non-linear in terms of the back relief: e.g., a small back narrow depression or a small particle very close to a larger one (cf. figure 2) will induce negligible or no additional deformation. Nevertheless, the convolution approach is expected to describe the main features, and can be accurate in certain cases, such as isolated particles for a semiconductor wafer, or a smooth and less structured back relief for the ancient mirror. It is also reasonable to state that for an arbitrary back profile, a corresponding profile exists for which the response is closely linear. The formula (7) cannot be applied directly as a convolution function, since the convolution would be dimensionally incorrect. It must be divided by the width squared to obtain the Gaussian like a probability density function. The convolution function will thus be:

$$g(x,y) = \frac{A}{2\pi d^2}\, exp\left(-\frac{x^2+y^2}{2d^2}\right). \quad (8)$$

The integral of $g(x, y)$ over the entire x-y plane is A. This quantity thus will have expressive meanings: A gives the specific volume of the material removed for a point-like back excitation (see figure 1(b) and figure 2) as well as the relative height response to a backside step, that is, the same meaning as in equation (7).

Now, we can write the expression for the resulting front relief h_f as

$$h_f(x,y) = -g(x,y) * h_b(x,y) \quad (9)$$

where h_b is the back relief (both measured outward the mirror plate). The negative sign expresses the fact that a back protrusion results in a depression in the front face. The objects we are dealing with are finite-sized and are closely planar, so heights at the periphery and outside the mirror area can be considered zero; and, as the Gaussian function extends to infinity, all convolution integrals are carried out over the whole x-y plane.

2.3 Effect of the backside pattern on the imaging

Now, if we substitute the expression (9) for h_f to equations (1) to (4), we obtain the imaging equations as a function of back relief (omitted here for simplicity).

The derivative theorem of convolution [23] states that, if u_1 or u_2 are integrable functions, then

$$\frac{\partial}{\partial x}(u_1 * u_2) = \left(\frac{\partial}{\partial x}u_1\right) * u_2 = u_1 * \left(\frac{\partial}{\partial x}u_2\right). \quad (10)$$

Applying this repeatedly on both x and y variables then using the distributive property of convolution we arrive at the following auxiliary expression:

$$\Delta(u_1 * u_2) = (\Delta\, u_1) * u_2 \quad (11)$$

For the gradient of a convolution,

$$grad(u_1 * u_2) = \left(\left(\frac{\partial}{\partial x}\, u_1\right) * u_2,\ \left(\frac{\partial}{\partial y}\, u_1\right) * u_2\right) \quad (12)$$

trivially holds. Utilising these, further operations can be carried out as will be detailed in the following sections. The commutativity of the convolution operation (interchangeability of u_1 and u_2) usually calls for different approaches.

3. Results and discussion

3.1 The general case

Exploring the overall properties of the imaging poses a methodological problem: because of the nature of the convolution, the properties of the imaging at a certain front surface point is determined by the properties not of the corresponding back surface point only, but by its adjacent convolution area (several times d). Therefore, we have the following options: *(i)* investigate the imaging equations using algebraic manipulations to find general features, *(ii)* studying the imaging of characteristic special back surface shapes, and

Accepted Manuscript

(iii) considering surface elements whose properties are constant over the convolution area.

The gradient change across the mirror surface (equation (1)) results in a topological mapping (distortion) of the mirror image, and the intensity profiles of a given surface feature is also affected by the local gradients. However, as discussed in Section 2.1, the intensity *value* pertinent to a given ***r*** point is not changed. It is difficult to assess how the convolution affects this mapping, since the convolution causes a change in the argument (***f***) of the function expressing the intensity (equation (2)). For the slowly varying gradient component, the smoothing effect of the convolution will be small; in other words, the pattern transfer process has no effect on the global shape of the mirror and the large-scale topological mapping.

Unfortunately, the Gaussian curvature term in the imaging equation prevents further manipulation or simplification, since in the expression of the Gaussian curvature, a product's members are convoluted first.

As for the option *(ii)*, a back surface feature described by a two-variable Gaussian function as follows is considered:

$$h_b = h_{b0}\, exp\left(-\frac{x^2}{2d_{b1}^2}-\frac{y^2}{2d_{b2}^2}\right). \quad (13)$$

Convoluting this with $-g(x, y)$, we obtain the front-face profile. After performing this convolution, we obtain a two-variable Gaussian depression as:

$$h_f = -Ah_{b0}\frac{d_{b1}d_{b2}}{\sqrt{(d_{b1}^2+d^2)(d_{b2}^2+d^2)}}\, exp\left(-\frac{x^2}{2(d_{b1}^2+d^2)}-\frac{y^2}{2(d_{b2}^2+d^2)}\right). \quad (14)$$

Substituting h_f into equation (2) we get the intensity profile. The H and K curvatures will then be:

$$H = \frac{C}{2}exp(\dots)\left[\frac{x^2-(d_{b1}^2+d^2)}{(d_{b1}^2+d^2)^2}+\frac{y^2-(d_{b2}^2+d^2)}{(d_{b2}^2+d^2)^2}\right] \quad (15)$$

and

$$K = C^2[exp(\dots)]^2\left[\frac{x^2-(d_{b1}^2+d^2)}{(d_{b1}^2+d^2)^2}\cdot\frac{y^2-(d_{b2}^2+d^2)}{(d_{b2}^2+d^2)^2}-\frac{x^2y^2}{(d_{b1}^2+d^2)^2(d_{b2}^2+d^2)^2}\right], \quad (16)$$

where C is the term in (14) before the exponential term and the exponential arguments are the same as in (14).

Particular interest is the behaviour at $x = y = 0$, at which the curvatures become:

$$H = -\frac{C}{2}\left[\frac{1}{d_{b1}^2+d^2}+\frac{1}{d_{b2}^2+d^2}\right] \quad (17)$$

and

$$K = C^2\,\frac{1}{(d_{b1}^2+d^2)(d_{b2}^2+d^2)}. \quad (18)$$

The degree of non-linearity (as defined in section 2.1) is (now resolving C):

$$-\frac{LK}{H} = -2LAh_{b0}\frac{d_{b1}d_{b2}}{\sqrt{(d_{b1}^2+d^2)(d_{b2}^2+d^2)}}\cdot\frac{1}{(d_{b1}^2+d^2)+(d_{b2}^2+d^2)}. \quad (19)$$

The focal distances f_D can be found either by solving $1/I = 0$ for L or directly as $f_D = 1/(2\mathrm{d}^2h_f/\mathrm{d}x^2)$ (and the same with y). (There are two focal distances due to the astigmatism of the reflected beam.) We obtain then at the origo:

$$f_{D_{1,2}} = \frac{d_{b1,2}^2+d^2}{2Ah_{b0}d_{b1}d_{b2}/\sqrt{(d_{b1}^2+d^2)(d_{b2}^2+d^2)}}. \quad (20)$$

Analysing the expressions above, we can conclude the following: The parameter A has a linear effect on h_f, and, consequently, on the slopes and curvatures. The convolution has a symmetrising effect in the in-plane directions: the ellipticity of the front surface shapes is reduced (a kind of "rounding" takes place characterised by d). The astigmatism of the reflected beam is also decreased. The nonlinearity is also reduced by increasing d (see equation (19)). Limiting cases are *(i)* $d << d_{b1,b2}$: the shape does not change significantly, only the multiplication by A remains, *(ii)* $d >> d_{b1,b2}$: the original front shape will be close to the convoluting Gaussian. The minimum width of the front depression is thus d; this limits the focal length to $d^2/(2Ah_{b0})$; astigmatism is removed.

The third approach is to consider an elemental second-order surface as

$$h_b = \frac{x^2}{2C_{min}}+\frac{y^2}{2C_{max}}. \quad (21)$$

Here $C_{min,max}$ are the two principal curvatures at the origo. This is a smooth surface whose curvatures are constant over the width of the convoluting Gaussian. The convolution by $-g(x, y)$ yields a simple result:

$$h_f = -Ah_b + const., \quad (22)$$

that is, the height, and also the shapes and curvatures are multiplied by $-A$. In fact, this corresponds to the $d << d_{b1,b2}$ case discussed above with the second order approximation of the Gaussian curve around the origo (cf. equation (13)). (The additive constant appears due to the integral but has no importance as the imaging are determined by derivatives.) The importance of this approximation is facilitating the tentative assessment of the saddle-shape regions as well, as it is not possible to construct a simple elementary surface which has saddle shape, yet integrates smoothly into an overall flat surface unlike a Gaussian as discussed above.

3.2 The linear case

Based on equations (3) (with $\boldsymbol{f}(\boldsymbol{r}) = \boldsymbol{r}$) and (11) we can write the imaging equation for the linear case in three alternative means:

$$1 - I(\boldsymbol{r})^{-1} = -2L\Delta\big(h_b(\boldsymbol{r}) * g(\boldsymbol{r})\big), \quad (23)$$

$$1 - I(\boldsymbol{r})^{-1} = -2Lh_b(\boldsymbol{r}) * \Delta g(\boldsymbol{r}) \quad (24)$$

and

$$1 - I(\boldsymbol{r})^{-1} = -2L\Delta h_b(\boldsymbol{r}) * g(\boldsymbol{r}). \quad (25)$$

Note that we used the transformed intensity $1–1/I$; with this, these equations without the linear approximation, also represent all surfaces where $K = 0$, that is, surfaces of translational symmetry. Each equation has different

Accepted Manuscript

interpretation. Equation (23) represents the image formation as described above: first, the back pattern is transferred by convolution to the front side, then the image is formed as described by the Laplacian. Equation (24) states that the image can be constructed by convoluting the *backside* relief with the Laplacian of the Gaussian (LoG) function. This is an interesting result as the front surface does not appear explicitly in the scenario. Figure 4 shows the plot of the LoG function (height A, width d). Interpreting this as (transformed) intensity profile we obtain the negative of the well-known image [5, 8-10, 21] (cf. also figure 1(c)) of a surface depression (or mound for negative L), which is the response to a backside point-like excitation. Finally, equation (25) expresses that the back relief is imaged *first* by the magic mirror principle than the resulting image is convoluted (smoothed) by the Gaussian. This might be against intuition, however the formula is valid only in the linear approximation.

The equivalence of these three formulae expresses the commutativity of the convolution and the Laplacian operations.

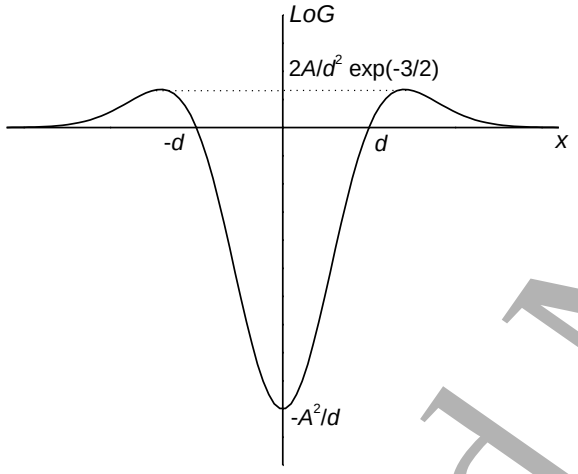

Figure 4. The plot of the Laplacian of the Gaussian (LoG) function

Berry has noted [3] the analogy between the edge detection [24] in digital image processing and the imaging of an abrupt backside step. Indeed, convolution by the LoG function is one basic algorithm of edge detection in digital images [25], where the role of the Gaussian is to smooth the step thus facilitating subpixel resolution and mitigate aliasing and noise effects. Our discussion goes further and extends this analogy that, based on equation (24), the magic mirror imaging can also be interpreted as a one-step process, the direct convolution by the LoG function, similarly to image processing where LoG is realised in a single step by the convolution of a matrix [25], whose elements' values follow the LoG function.

3.3 Diffraction effects

The minimum width of bright patches in the image are limited by diffraction as they result in by focusing by a finite surface area of the mirror. It has been suggested that this effect limits the lateral resolution of the imaging [22]. The effect can be quantified approximately as follows. The diffraction-limited diameter or width of the bright patch in general is given by

$$\delta = 2.44\lambda \frac{f_D}{D}, \qquad (26)$$

where f_D is the focal length and D is the diameter (or width) of the focusing area and λ is the illuminating wavelength. For a straight element, the constant 2.44 is replaced by 2. The focal length f_D is calculated as described in section 3.1. We take the focal point at the minimum of the second derivative as above this we enter into the caustic region of imaging. Now consider focusing by a Gaussian (circular or straight geometry) depression and a smoothed step (error function) as these are the basic elements of a surface topography and represent somehow limiting cases. A Gaussian protrusion is also considered; it cannot be formed naturally, however it is equivalent to a depression imaged with negative L.

To find D for the Gaussian depression, we take the convex part of the Gaussian whose width is $D = 2d$. The focal length will be $d^2/(2h_0)$, where h_0 is the height of the Gaussian. The diffraction-limited diameter will thus be $0.61\lambda(d/h_0)$. For the Gaussian protrusion, the side tails will focus. It is somehow arbitrary to determine the value of D since the tails extend to infinity with decreasing slope, but d is a good estimate (see figure 3). The focal length will be $1.12d^2/h_0$, thus we obtain $\delta = 2.24\lambda(d/h_0)$ (using the straight case for equation (25)). For the straight edge, the second derivative is the Gaussian; we can again take $D = 2d$, the focal length will be $2.1d^2/h_0$ thus we obtain $\delta = 2.1\lambda(d/h_0)$; here h_0 is the step height.

In summary, the diffraction-limited minimum size of the bright patches is roughly $\delta = c\,\lambda(d/h_0)$, where the c proportionality constant is in the order of unity (roughly 0.5 to 2), depending on the actual surface profile. For semiconductor wafers, taking d = 1 mm, h_0 = 1 μm [20] and c = 1 we get f_D = 1 m and δ = 0.5 mm for visible light (λ = 0.5 μm). We expect similar values for the ancient mirror, since d (two times mirror thickness, see section 2.2) and front relief range values are in the similar range [22]. It is also likely that the lack of the sharp focus due to diffraction is partly responsible for the large "depth of field" of the ancient mirrors noted by several authors [4].

3.4 Concluding remarks on imaging

Finally, we make a remark on Gitin's model [4]. The author raised the question: under what circumstances can a magic mirror perform an optical imaging, that is, produce an image where the intensity at a point is proportional to the height elevation of the corresponding point of the back surface? Gitin's answer was that the point spread function (intensity distribution for a back impulse excitation) should be close to

Accepted Manuscript

the Dirac delta, and this happens when the screen is in the focus of the Gaussian front-face depression resulting from the impulse, that is in our notation: $L = d^2/(2h_0)$. We have seen that this never happens (not even in the linear approximation Gitin applied), as the bright focus spot is surrounded by a dark ring. In fact, this is generally true for depressions of any shape. The response of the system without excitation (that is, flat back and front face) is a uniform intensity of $I = 1$. If a finite-size front depression produces a bright spot ($I > 1$) in the image by focusing, the flux conservation requires that there must be dark areas ($I < 1$) within the image of the depression area.

4. Conclusion

The effects of backside pattern transfer in magic-mirror imaging was modelled using a convolution approach. Global features were inferred and the linear approximation was discussed in detail, compared to earlier models. Our results may have relevance in other areas of optics. It has been suggested by several authors [4, 26, 27] that Makyoh is a special kind of 'optical processing element' where a wavefront is modified by the sub-wavelength relief of a globally planar reflecting surface. This approach leads to the realm of freeform optics where Laplacian or magic-mirror imaging is often referenced [21, 28].

References

[1] Saines G and Tomilin M G 1999 Magic mirrors of the Orient *J. Opt. Technol.* 66 758–65.

[2] Thompson S P 1893 Ye magick mirrour of old Japan, London, private edition.

[3] Berry M V 2006 Oriental magic mirrors and the Laplacian image *Eur. J. Phys.* 27 109–18

[4] Gitin A V 2009 System approach to image formation in a magic mirror Appl. Opt. 48 1268–73

[5] Riesz F 2000 Geometrical optical model of the image formation in Makyoh (magic-mirror) topography *J. Phys. D: Appl. Phys.* 33 3033–40

[6] Teoh Eden Kang Min, May Watt Sook, Sreemathy Parthasarathy, Huang Lei, Asundi Anand 2013 Investigation of surface & sub-surface profile, techniques of measurement and replication of the Chinese magic mirror *Proc. SPIE* 8769 876930-1

[7] Seregin D A, Seregin A G and Tomilin M G 2004 Method of shaping the front profile of metallic mirrors with a given relief of its back surface J. *Opt. Technol.* 71 121–2

[8] Tokura S, Fujino N, Ninomiya M, Masuda K 1990 Characterization of mirror-polished silicon wafers by Makyoh method *J. Cryst. Growth* 103 456–60

[9] Okabayashi O, Shirotori H, Sakurazawa H, Kanda E, Yokoyama T, Kawashima M 1990 Evaluation of directly bonded silicon wafer interface by the magic mirror method *J. Cryst. Growth* 103 437–442

[10] Lazareva I, Nutsch A, Pfitzner L, Frey L 2010 Optical inspection of flat reflective surface by a wave front sensor *Proc. SPIE* 7792 77920Q-1

[11] Taklo M M V, Storås P, Schjølberg-Henriksen K, Hasting H K, Jakobsen H 2004 Strong, high-yield and low-temperature thermocompression silicon wafer-level bonding with gold *J. Micromech. Microeng.* 14 884–90

[12] Vinothkumar S, Sathyan Subbiah Sankaran S 2020 Subsurface pore-induced quilting during machining of metal foams *J. Micro- and Nano-Manufacturing* 8 024509

[13] Hibino K, Yamauchi M, Katoh M and Matsuda K 1990 Modern technique for the production and measurement of Makyoh images *J. Cryst. Growth* 103 433–6

[14] Kawai R, Aoyama E, Hirogaki T, Ogawa K, Sawa K 2012 Surface generation for Magic-Mirror by end-milling and magnetic polishing with digitally functioned CNC machining center *Key Engineering Materials* 523-524 368–73

[15] Adnana A S, Ramalingama V, Kob J H, Subbiaha S 2014 Nano texture generation in single point diamond turning using backside patterned workpiece *Manufacturing Letters* 2 44–8

[16] Chu Kwang-Hua A 2006 Comments on 'Oriental magic mirrors and the Laplacian image' *Eur. J. Phys* 27 L13–5

[17] Riesz F 2013 Non-linearity and related features of Makyoh (magic-mirror) imaging *J. Opt.* 15 075709.

[18] Riesz F 2006 A note on 'Oriental magic mirrors and the Laplacian image' *Eur. J. Phys.* 27 N5–7.

[19] Koroyasu S, Kubo K, Asao H, Shioya T, Matsuda M 2011 Magic mirror phenomenon caused by metal shrinkage in solidification and cooling process (examination by thermal elasto-plastic deformation analysis) *Proc. Japan Society of Mechanical Engineers*, Kanto Branch Block Joint Lecture, Utsunomiya, p. 133.

[20] Bearda T, Mertens P W, Holsteyns F, De Bisschop P, Compen R, Van Meer A, Heyns M M 2005 The effect of backside particles on substrate topography *Japan. J. Appl. Phys.* 44 7409–13

[21] Wooyoun Kim, Cassarly B, Rolland J P 2021 Connecting tolerancing of freeform surface deformation in illumination optics with the Laplacian magic mirror *Optics Express* 29 40559

[22] Gamo H 1984 Imaging optics of a Japanese magic mirror *13th Congress Int. Commission for Optics*, 20–24 August, 1984, Sapporo, pp. 348–9

[23] Bracewell R N 2000 The Fourier transform and its applications, McGraw-Hill: Boston, p. 126.

[24] Marr D and Hildreth E 1980 Theory of edge detection *Proc. R. Soc. B* 207 187–217.

[25] Sotak G E, Jr. Boyer K L 1989 The Laplacian-of-Gaussian kernel: a formal analysis and design procedure for fast, accurate convolution and full-frame output *Computer Vision, Graphics, and Image Processing* 48 147–89

[26] Kovatchev M, Ilieva, R 1996 Diffractive, refractive optics or anything more? Comparative analysis and trends of development, *J. Modern Optics* 43 1535–41

[27] Smolovich A M 2006 Achromatic optical elements *Appl. Opt.* 45 7871–7

[28] Bawart M, Bernet S, Ritsch-Marte M 2017 Programmable freeform optical elements *Optics Express* 25 4898

Accepted Manuscript